Silver nanoparticle embedded copper oxide as an efficient core–shell for the catalytic reduction of 4-nitrophenol and antibacterial activity improvement

Nabil Bouazizi, Julien Vieillard, P. Thebault, F. Desriac, T. Clamens, Radhouane Bargougui, N. Couvrat, Olivier Thoumire, N. Brun, Guy Ladam, et al.

HAL Id: hal-02337263

https://hal.science/hal-02337263

Submitted on 29 Oct 2019

Check for updates

Dalton Transactions

Accepted Manuscript

Volume 45 | Number 1 | 7 January 2016 | Pages 1–398

Dalton Transactions

An international journal of inorganic chemistry
www.rsc.org/dalton

ISSN 1477-9226

PAPER
Joseph T. Hupp, Omar K. Farha et al.
Efficient extraction of sulfate from water using a Zr-metal–organic framework

175 YEARS
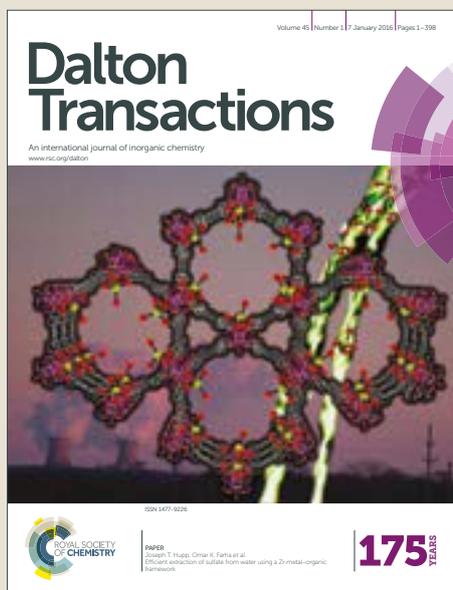
ROYAL SOCIETY OF CHEMISTRY

rsc.li/dalton

Silver Nanoparticles Embedded Copper Oxide as Efficient Core-Shell for Catalytic Reduction of 4-nitrophenol and Antibacterial Activity improvements

Bouazizi, N. [a]; Vieillard, J. [a*]; Thebault, P. [b]; Desirac, F. [c]; Clamens, T. [c]; Bargougui, R. [a];
Couvrat, N. [d]; Thoumire, O. [e]; Brun, N [e.] ; Ladam, G. [e]; Morin, S. [e]; Mofaddel, N. [a];
Lesouhaitier, O. [c]; Azzouz, A. [d*]; Le Derf, F. [a]

[a] Normandie Univ, UNIROUEN, INSA Rouen, CNRS, COBRA (UMR 6014), 55 rue saint Germain, 27000 Evreux, France
[b] Normandie Univ, UNIROUEN, CNRS, PBS (UMR 6270), Bâtiment Pierre-Louis DULONG, Bd Maurice de Broglie, F-76821 Mont Saint Aignan Cedex, France
[c] Laboratoire de Microbiologie Signaux et Microenvironnement (LMSM), EA 4312 IUT Evreux, 55, Rue Saint Germain, 27000 Evreux, France
[d] Normandie Univ, UNIROUEN, SMS EA 3233, rue Tesnière, 76000 Mont Saint Aignan, France
[e] Normandie Univ, UNIROUEN, CNRS, PBS (UMR 6270), centre universitaire, 1 rue du 7ème chasseur, 27000 Evreux, France
[d] Nanoqam, Department of Chemistry, University of Quebec at Montreal, QC H3C 3P8, Canada

*CORRESPONDING AUTHOR. Dr. J.Vieillard, Email: julien.vieillard@univ-rouen.fr;
Pr. A. Azzouz, E-mail addresses: azzouz.a@uqam.ca

Abstract

A facile and eco-friendly method was developed to prepare microporous $CuO@Ag^0$ core-shell with high catalytic and antibacterial activities. Scanning and transmission electron microscopy revealed a preponderance of nearly spherical 50 nm particles with slight structure compaction. Comparison of the hysteresis loops confimed the structure compaction after AgNP incorporation, and a significant decrease of the specific surface area from 55.31 m^2/g for CuO to 8.03 m^2/g for $CuO@Ag^0$ was noticed. Kinetic study of 4-nitrophenol (4-NP) reduction into 4-aminophenol (4-AP) by sodium borohydride revealed a first order reaction that produces total conversion in less than 18 minutes. $CuO@Ag^0$ also exhibited appreciable antibacterial activity against *Staphylococcus aureus*. The antibacterial effects were found to strongly depend on the size, contact surface, morphology and chemical composition of the catalyst particles. Addition of Ag^0-NPs produced more reactive oxygen species in the bacteria

medium. These results open promising prospects for potential applications as low cost catalyst in wastewater treatment and antibacterial agent in cosmetics.

Keywords: CuO@Ag^0; antibacterial activity; catalytic properties; nitrophenol conversion

1. Introduction

Water pollution is a major and vital environmental issue, and it is estimated that more than 50% of the countries will face water crisis by 2025 [1]. The control of water pollution has become one of the major challenges to be addressed worldwide. Among the wide variety of water pollutants, bacterial pathogens such as *Escherichia coli* and *Staphylococcus aureus* [2, 3], 4-nitrophenol (4-NP) and its derivate [4] are particularly hazardous for biodiversity and humain health. 4-NP is recognized as being very toxic, but its chemical conversion into less harmful derivative such as 4-aminophenol (4-AP) could be beneficial for water treatments. This avenue could be even more interesting, given that 4-AP can act as corrosion inhibitor, drying agent and antipyretic drugs [5, 6].

Water treatments involved so far numerous technologies including both physical and chemical processes [7]. Some of these processes may involve nanotechnology and nanomaterials as coagulant-floculents, adsorbents and/or catalysts [8] [9], and some of them already turned out to be promising materials for environmental applications [10]. The physicochemical properties of such materials are strongly dependent on their structure, morphology and specific surface area [11]. Among the wide variety of materials used or investigated in this regard, metal oxides such as TiO_2, ZnO, NiO, Fe_2O_3 and more particularly CuO are of great interest for some environmental purposes [12]. Reportedly, CuO-based materials were already found to exhibit catalytic and antibacterial activities [13]. CuO can be prepared through various methods such as chemical vapor deposition, hydrothermal method, and sol-gel process [14-16]. The hydrothermal method appears as the simplest and lowest cost route for the synthesis of CuO nanoparticles. The catalytic and antibacterial properties of CuO

can be induced and enhanced through some judicious modification procedures. CuO combinations with metals or metal oxides such as $CuO-SnO_2$, Ag/CuO and CuO-ZnO were already found to show activity against gram negative bacteria, and incorporation of metal nanoparticles (MNP) such as silver is now recognized to induce antimicrobial activity [17, 18].

This is why a special interest was devoted to Ag nanoparticles (AgNP). In this regard, we developed a convenient and low cost route to synthesize a promising $CuO@Ag^0$ core-shell material. The properties of the as-prepared materials were correlated to its surface properties and performances as catalysis and antibacterial agent. The reduction of 4-NP to 4-AP by $NaBH_4$ was used as probe reaction, the catalytic activities of CuO and $CuO@Ag^0$ were evaluated and the kinetic parameters assessed. In the meantime, the in-vitro antibacterial activity of both CuO and its modified counterpart against *Staphylococcus aureus* were investigated.

2. Experimental

2. 1. Chemicals and material synthesis

In this research, one used copper (II) sulfate pentahydrate ($CuSO_4$), sodium hydroxide (NaOH), absolute ethanol (EtOH), silver nitate ($AgNO_3$), polyvinylpyrrolidone (10000 g.mol^{-1}, PVP), sodium tetrahydroborate ($NaBH_4$) and 4-Nitrophynol (4-NP).

Copper oxide nanoparticles was prepared by dissolving 1 g of $CuSO_4$ diluted in 100 mL of distilled water under vigorous stirring at 50°C until total dissolution. The resulting solution was then treated with 0.5g of NaOH under stirring and kept at 80 °C for 4 h. After cooling down to room temperature, the black precipitate was filtered, repeatedly washed and then dried at 90 °C overnight.

Further, $CuO@Ag^0$ core-shell was synthesized by coating the prepared CuO as core with Ag as shell. In this regard, 0.2g of CuO was dispersed in 40 mL aqueous solution under

vigorous stirring for 30 min. Ag^+ solution was prepared by dissolving 0.02g of $AgNO_3$ as precursor and 0.001 g of PVP as stabilizing agent in distilled water, and was then mixed with the aqueous CuO suspension and 5 mL of $NaBH_4$ solution under vigorous stirring at 25°C for 2 hours. The color of the mixture turned golden brown, indicating the reduction of the Ag^+ ions into metallic silver (Ag^0). The resulting $CuO@Ag^0$ material was separated by filtration, washed with distilled water and ethanol and further dried overnight at 80 °C **(Scheme 1)**.

Dalton Transactions Accepted Manuscript
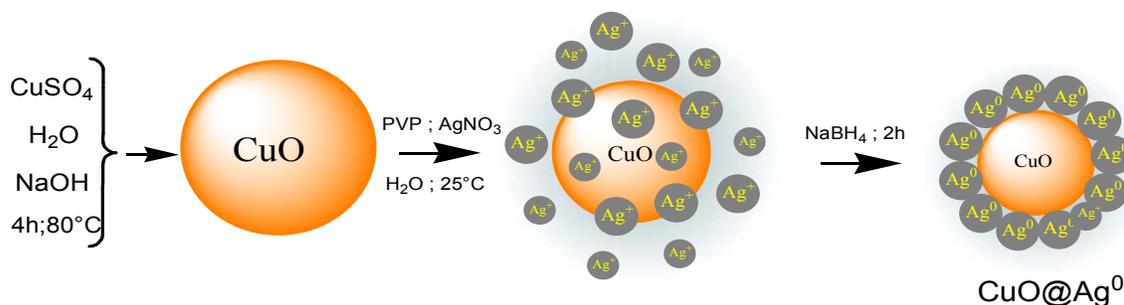
Scheme 1. Synthetic route for $CuO@Ag^0$ core-shell.

2.2. Material characterization

The material samples were characterized through Fourier transform infrared spectroscopy using a Tensor 27 (Bruker) spectrometer with a ZnSe ATR crystal. For each spectrum, 20 scans were accumulated with a resolution of 4 cm^{-1}. The particle morphology was investigated by Scanning Electronic Microscopy (SEM) by means of a ZEISS EVO 15 electron microscope, where samples were metallized by gold layer at 18 mA during 360 s with a Biorad E5200 device. Two types of images were acquired: secondary ion images to observe the morphology of the surface, and EDX images to evaluate the chemical contrast. The zeta potential was measured for each sample dispersion with the phase analysis light scattering mode (PALS) using a Malvern zeta sizer nanoZS setup. Sample dispersions were prepared from 2 mg of sample dispersed in 10 mL of deionized water and ultrasonicated during 15 minutes. Atomic Force Microscopy (AFM) images were acquired by means of a Dimension-3000 (Digital Instrument) microscope in the "light" tapping mode C = 0.292 N/m, with a scan rate 0.5 to 1 Hz. For the sample preparation, a drop of microcapsule suspension was placed onto a pre-cleaned and previously air-dried glass plate.

2.3. Catalytic activity

The catalytic activity of CuO and CuO@Ag^0 nanoparticles in the reduction reaction of 4-nitrophenol (4-NP) to 4-aminophenol (4-AP) was studied through UV–Vis spectrophotometric analysis of periodical samples taken from the reaction mixture using PELambda 650 Perkin-Elmer instrument, using distilled water as a reference solution. The catalytic test were carried out in a 1 cm quartz cell by mixing 1 mL of aqueous solutions of NaBH$_4$ (1 mL, 0.2 M) and 4-NP (2 mL, 2.5 mM) with various amounts of CuO or CuO@Ag^0 (5-20 mg). The presence of 4-AP was confirmed by color change of the reaction mixture. Upon addition of NaBH$_4$, the color of the aqueous solution of 4-NP changed from light yellow to dark yellow, indicating the formation of 4-nitrophenolate ions [19]. During the reaction, the solution turned colorless due to the formation of 4-AP (**Scheme S1**).

2.4. Antibacterial activity

The antibacterial activity of CuO and CuO@Ag^0 nanoparticles was investigated using a *Staphylococcus. aureus (ATCC 29213)* strain, previously maintained as glycerol stocks and stored at -20 °C. Precultures were performed for 18 h in Brain Heart Infusion. For this purpose, Minimal Inhibitory Concentration (MIC) measurements were made through microdilution method based on ISO standard 20776-1 (Ref: International Organization for Standardization (ISO). ISO 20776-1, 2007, 19 pp). MIC is defined as the lowest concentration of core-shell that inhibits the visible bacterial growth after overnight incubation. In this regard, a dispersion of each material at various concentrations like 12; 25; 50; 75; 100; 125; 150 and 200 µg.mL^{-1} in a mixture of PBS/BHI (50/50; v/v) was inocculated by a bacterial suspension (around 10^{5-6} colony forming units CFU.mL^{-1}). Positive and negative controls were included in each assay. After 24 h of incubation at 37°C on a Dynabeads ® MX1-Mixer (from Invitrogen) at 30 rpm, the bacterial growth was visualized by the broth turbidity for each solution.

3. Results and discussion

3.1. Particle size and morphology

A quick overview with an optical microscopy (**Fig. S1**) revealed aggregated CuO particles (**1**), most likely due to the occurrence of strong interaction through H-bridges between terminal hydroxyl groups. High dispersion was noticed after AgNP incorporation (**2**), which can be explained in terms of the appearance of competitive Ag^0:O(H)Cu interaction at the expense of H-bridges (2). This confirmed by AFM images, with showed the higher dispersion grade of CuO@Ag as compared to CuO (**Fig S2**).

SEM images (**Fig. 1**) showed flock-shaped CuO particles (*a*), which transformed into compacted pseudo-spheres upon AgNP incorporation. A non-uniform distribution of the particle size varying between 200 and 700 nm was noticed for CuO@Ag^0 core-shell material (**Fig. S3**). This must be due to electrostatic interaction between terminal hydroxyl groups of CuO and AgNPs.

(a)
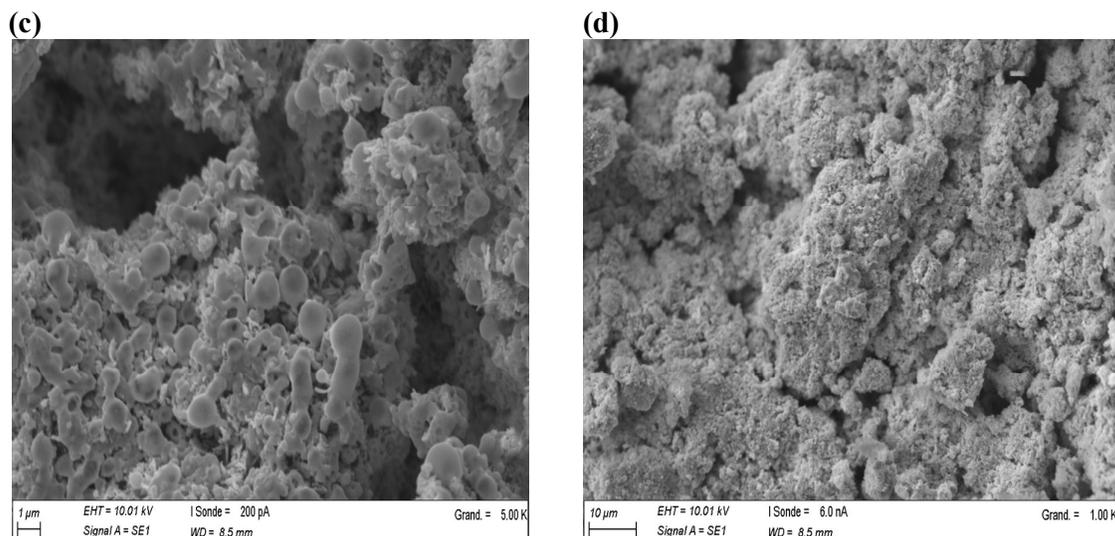
(b)
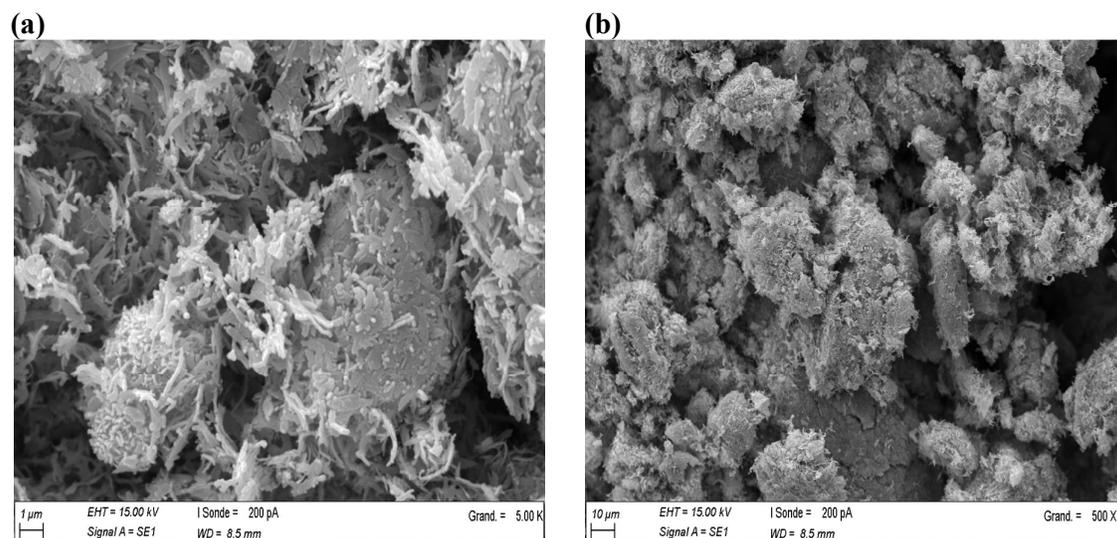
Fig. 1. SEM image of synthesized CuO (a, b) and CuO@Ag^0 (c, d).
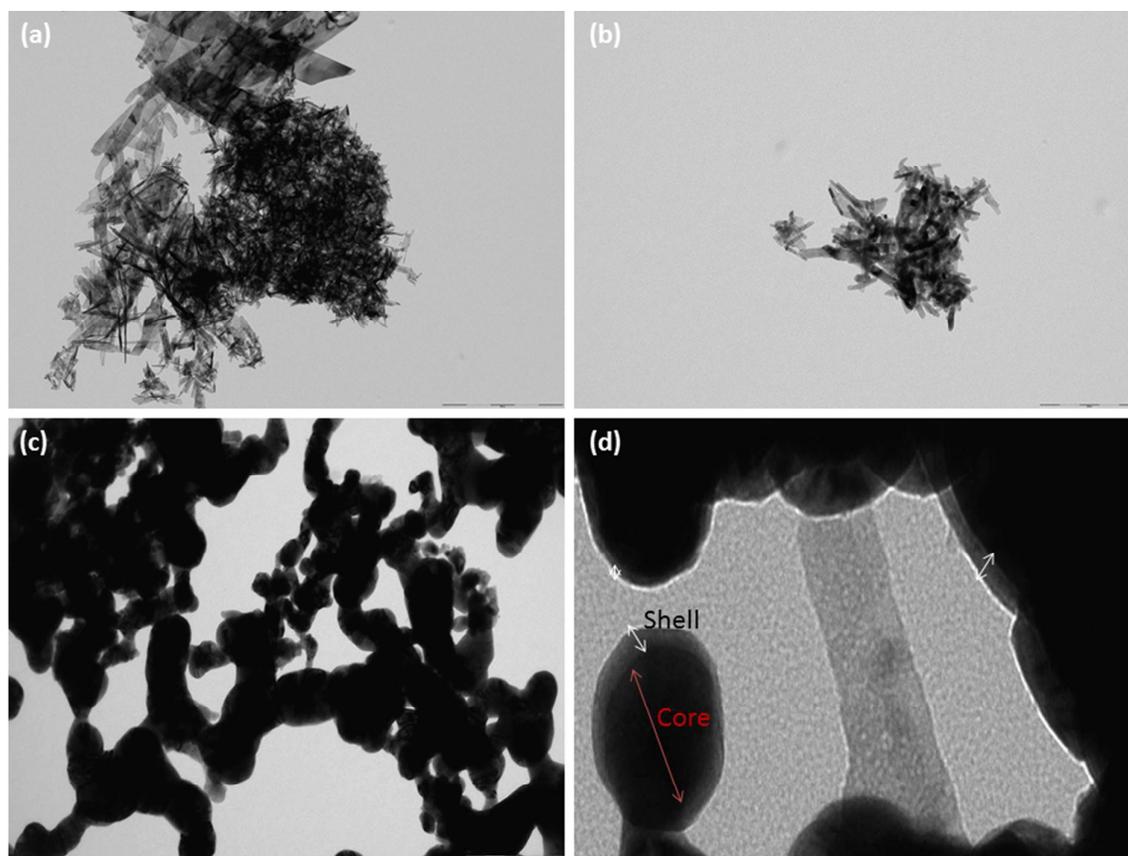

Fig. 2. TEM image of synthesized CuO (a, b) and CuO@Ag^0 (c, d).

The surface morphologies of both CuO and CuO@Ag samples were investigated using transmission electron microscopy (**Fig.2**). **Fig. 2-**a is the image of CuO, which can be seen that morphologies of the CuO nanoparticles are in sheet shape and uniform. This was in good agreement with those obtained by SEM analysis. The size of nanoparticles is approximately 600 nm, also in accordance with the SEM analysis. However, clearly show the existence of Ag nanoparticles. After encapsulation with Ag nanoparticles, visible changes are marked on the morphology of CuO@Ag. Clearly the CuO nanoparticles are intimately covered by Ag nanoparticles, producing a shell on the CuO surface. Thus, core-shell structure of CuO@Ag was successfully obtained. The average of the shell thicknesses is around 10nm, as supported in **Fig. 2**. The CuO sheets core appears black and Ag shell was with light colored in the image, due to the higher mass thickness contrast of CuO nanoparticles. This structure would be expected to supply new active sites and significantly promote mass and electron transfer for antibacterial and catalytic activities. To confirm the core-shell structure of the nanoparticles more distinctly, the EDX line scanning was conducted.

EDX spectroscopy confirmed the presence of AgNPs (**Fig. S4**). Measurements using a Zetasizer instruments revealed a structure compaction after AgNP incorporation, presumably due to sufficiently strong interaction Ag:O(H)-CuO. This was supported by a noticeable decrease of the average particle diameter from 1020-1800 nm for CuO to ca. 400-520 nm for CuO@Ag^0 (**Fig. S3**) in agreement with SEM data.
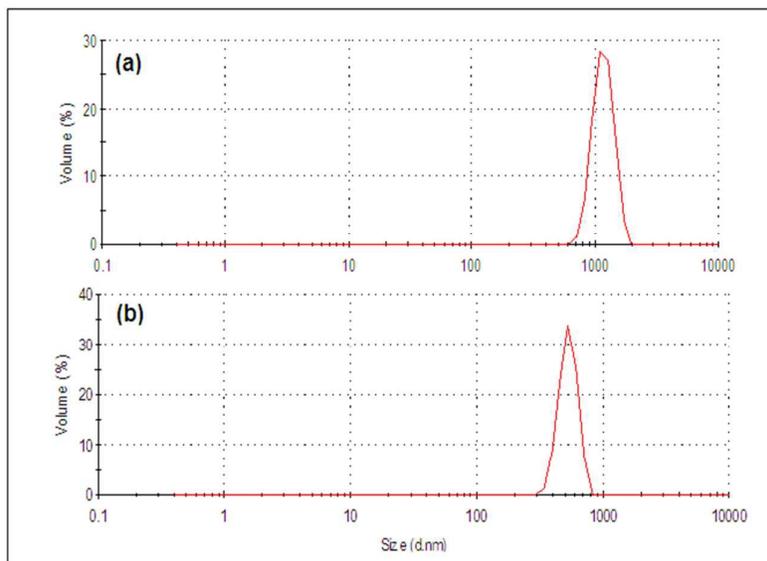
Fig. 3. Zetasizer of CuO (a) and CuO@Ag^0 (b).

3.2. Textural features

N_2 adsorption–desorption cycles performed at 77 K of CuO and CuO@Ag^0 (**Fig. 4**)

revealed a type IV isotherm accompanied by an H3-type hysteresis loop for mesoporous

materials defined by IUPAC classification. Comparison of the hysteresis loops confimed the

structure compaction after AgNP incorporation, and a significant decrease of the specific

surface area (SSA) from 55.31 m^2/g for CuO to 8.03 m^2/g for CuO@Ag^0 was noticed.
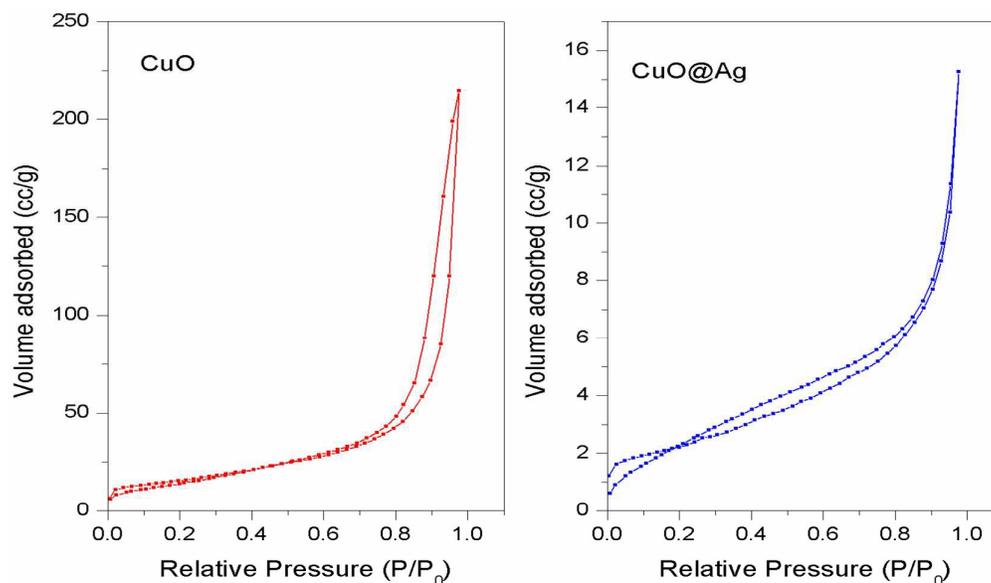
Fig. 4. Nitrogen adsorption-desorption isotherms of CuO and CuO@Ag^0.

This was accompanied by a marked decay in porosity, inasmuch as the micropores volume

dramatically dropped from 0.124 cc/g down to an almost ten times lower values of 0.013 cc/g.

These results are in agreement with the microposcopy analysis data.

3.3. Structural changes upon AgNPs incorporation

The composition and structural properties were examined by powder X-ray diffractometry.

Figs. S5 showed the XRD pattern of CuO and CuO@Ag nanoparticles. All the diffraction

peaks are in good correlation with bulk orthorhombic (Card No. 01-077-1898) CuO. The

observed patterns are cross-matched with those in the JCPD database. The diffraction peaks

of the impurity are not found in the XRD patterns, proving that the synthesized products have

high purity. The diffraction peaks of CuO are found at 2θ values of 33.5, 36.0, 39.2, 49.4,

52.8 and 59.3, referring to diffraction from (1 1 0), (−1 1 1), (1 1 1), (−2 0 2), (0 2 0), and (2

0 2) planes, respectively, for the cubic phase. In the XRD pattern of the as-synthesized

CuO@Ag sample, the coexistence of CuO and Ag was confirmed, by the new peaks appeared

at 39.5 and 43.9, which corresponded to (1 1 1) and (2 0 0) planes of silver with face-

centered-cubic phase.

On the other hand, a visible structural change are noticed, which resides in the marked

decay of the Zeta potential (ZP) as measured in aqueous dispersions of CuO and CuO@Ag

below pH 6 (**Fig 5**). This effect must be due to the conductivity of AgNPs, and seems to be

progressively attenuated with increasing pH. Both CuO and CuO@Ag^0 showed negative and

close values for pH > 6.
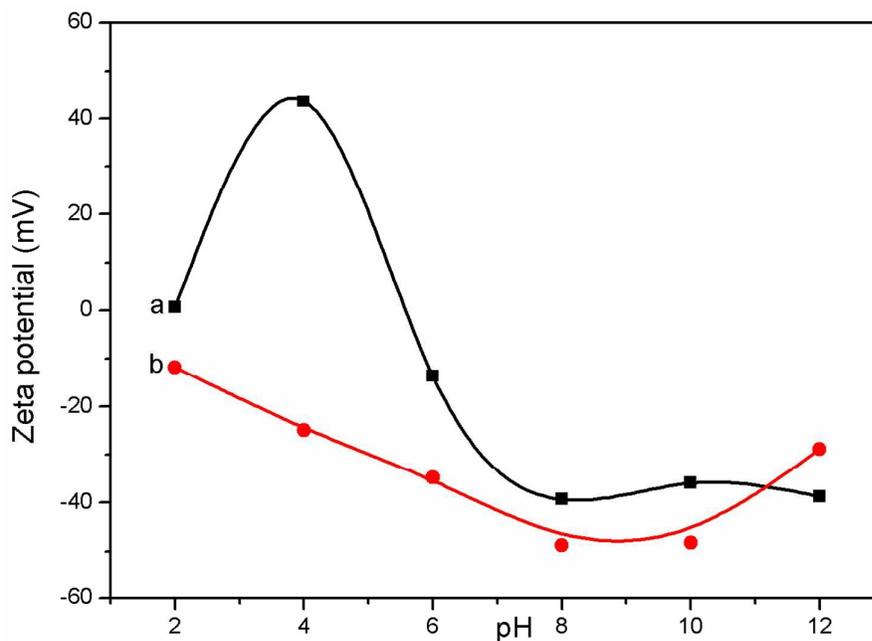
Fig. 5. Zeta potential of CuO (a) and CuO@Ag^0 (b) for different pH values.

The fact that CuO@Ag^0 displays negative Zeta potential in the entire pH range indicates a higher and more stable dispersion as compared to CuO. Even though this is a special feature of improved repulsion between similarly charged particles of metal loaded oxide [20, 21], this must be mainly due to the disappearance of H-bridges between the particles as a result of the involvement of terminal OH groups of CuO in Ag:OH- interaction, as previously stated.

3.4. Thermal analysis

DSC analysis showed an endothermic peak between 50 and 100°C for CuO mostly due to dehydration (**Fig. 6**). This peak totally disappeared upon AgNP incorporation, indicating a significant decay of the hydrophilic character, presumably as a result of the rise of Ag^0:OH- interaction. The latter is supposed to induce a depletion of free OH groups at the expense of H-bridges between water and terminal OH groups [22]. This result is a precise index of the key-role of hydroxyls in the stabilization of AgNPs.
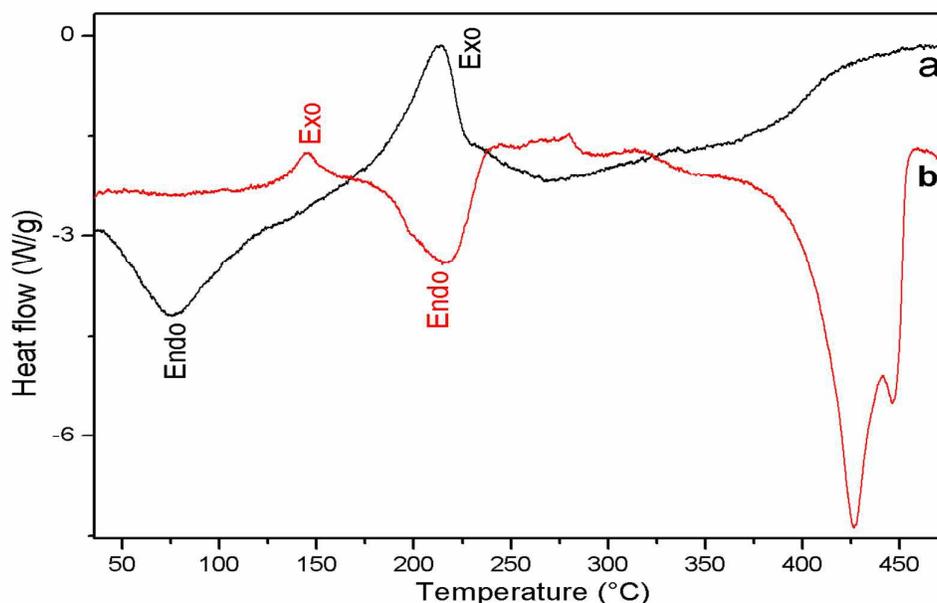
Fig. 6. DSC curves of CuO (a) and CuO@Ag^0 (b).

The presence of exothermic peaks for both CuO and CuO@Ag^0 at ca. 212°C and 140°C, respectively, indicates the occurrence of so-called thermite processes [23]. Such processes involve pyrotechnic reactions between metals and their impurities and/or metal oxide powders. The conversion of the exo peak of CuO into an endo process and a lower intensity exo one must be due to CuO dehydroxylation and the formation of Cu-O-Ag bonds. The strong endothermic peak noticed for CuO@Ag^0 around 430°C must be associated to AgNP sintering. The fact that this process is triggered much below the melting point of silver (961,8 °C) must be due the high dispersion of AgNPs [24]. Thus one may conclude that a thermal stability up 130°C allows using CuO@Ag^0 in catalysis and surface phenomena below this temperature threshold.

3.5. FT-IR analysis

The 605 cm^{-1} IR band associated to the Cu-O stretching vibration (**Fig. 7**) confirmed the formation of CuO phase [25]. The OH stretching vibration at approximately 3470 cm^{-1} attributed to the presence of terminal hydroxyl groups (−OH) [26] is a confirmation in this

regard. As expected and in agreement with previous statement, this band totally disappeared after AgNP incorporation, most likely due to the rise of Ag:OH- interaction. However, new peaks at 1652, 1471 cm^{-1} and 1136 cm^{-1} are associated to the bending vibration of C=O and C–O single bond coming from the PVP adsorbed to silver particles respectively [27]. The occurrence of a 820 cm^{-1} band was associated to Ag–O stretching vibration, and suggests an oxidation of Ag, presumably due to thermite processes between CuO and Ag. The shift of the 605 cm^{-1} IR band from 605 cm^{-1} to 403 cm^{-1} and the dramatical decay in intensity agrees with the already suggested rise of strong Ag:OH- interaction [28].
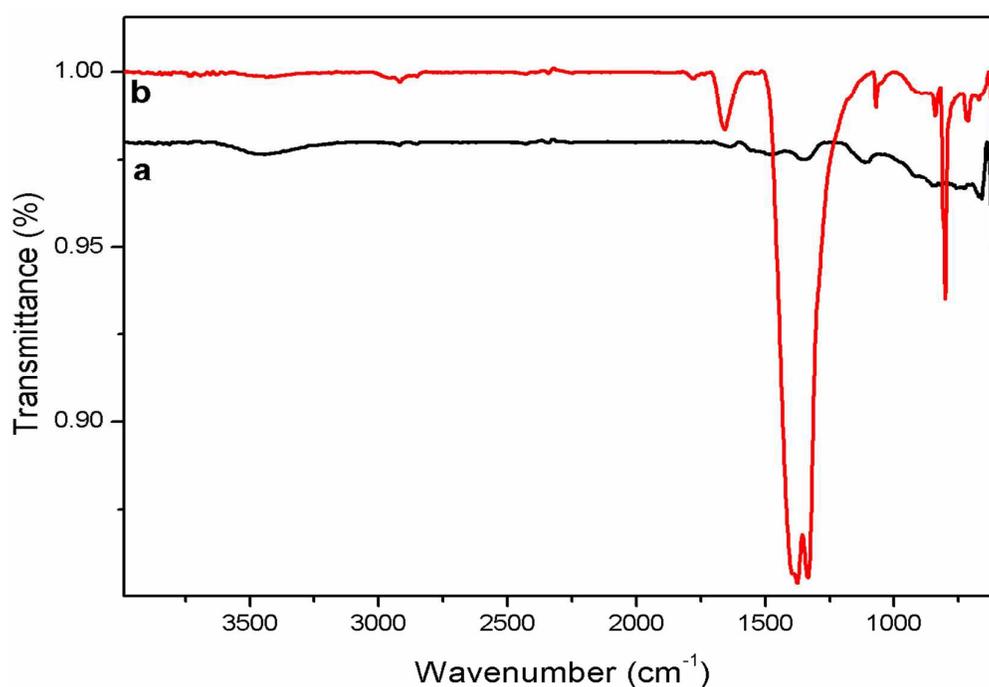
Fig. 7. FT-IR spectra of CuO (a) and CuO@Ag^0 (b).

3.6. Catalytic activity

The catalytic activity of both CuO and CuO@Ag^0 in 4-NP reduction was assessed through UV-Vis spectrophotometry (**Fig.8**). Preliminary tests without catalyst revealed a quick intensity decrease of the 400 nm band attributed to 4-NP, and a fast increase in intensity of the new peak at 290 nm indicates the formation of 4-aminophynol (4-AP) at the expense of 4-NP

through the action of NaBH$_4$ [29, 30]. This was accompanied by color changes from light

yellow to dark yellow and then to uncolored in the reaction mixture **(Fig. S6**). Here, it is

worth mentioning that though the reduction of 4-NP to 4-AP by NaBH$_4$ is thermodynamically

favorable, the presence of a kinetic barrier due to large potential difference between donor and

acceptor molecules should be detrimental [30]. The effect of CuO addition was confirmed by

stronger intensity decay of the 400 nm band for 4-NP and intensity increase of 290 nm peak

for 4-AP (**Fig. 8**). This effect was even more pronounced in the presence of CuO@Ag^0, which

provides evidence of the beneficial contribution of Ag^0 incorporation. This reaction

enhancement must be due to a key-role of both CuO and AgNPs in improving the electron

transfer from BH$_4^-$ ions to the nitro group of 4-NP [31]. Deeper insights in this regard were

achieved with different amounts of catalysts. A first overview of the results obtained revealed

that increasing catalyst concentration induces an acceleration of 4-NP reduction (**Fig. 8**).
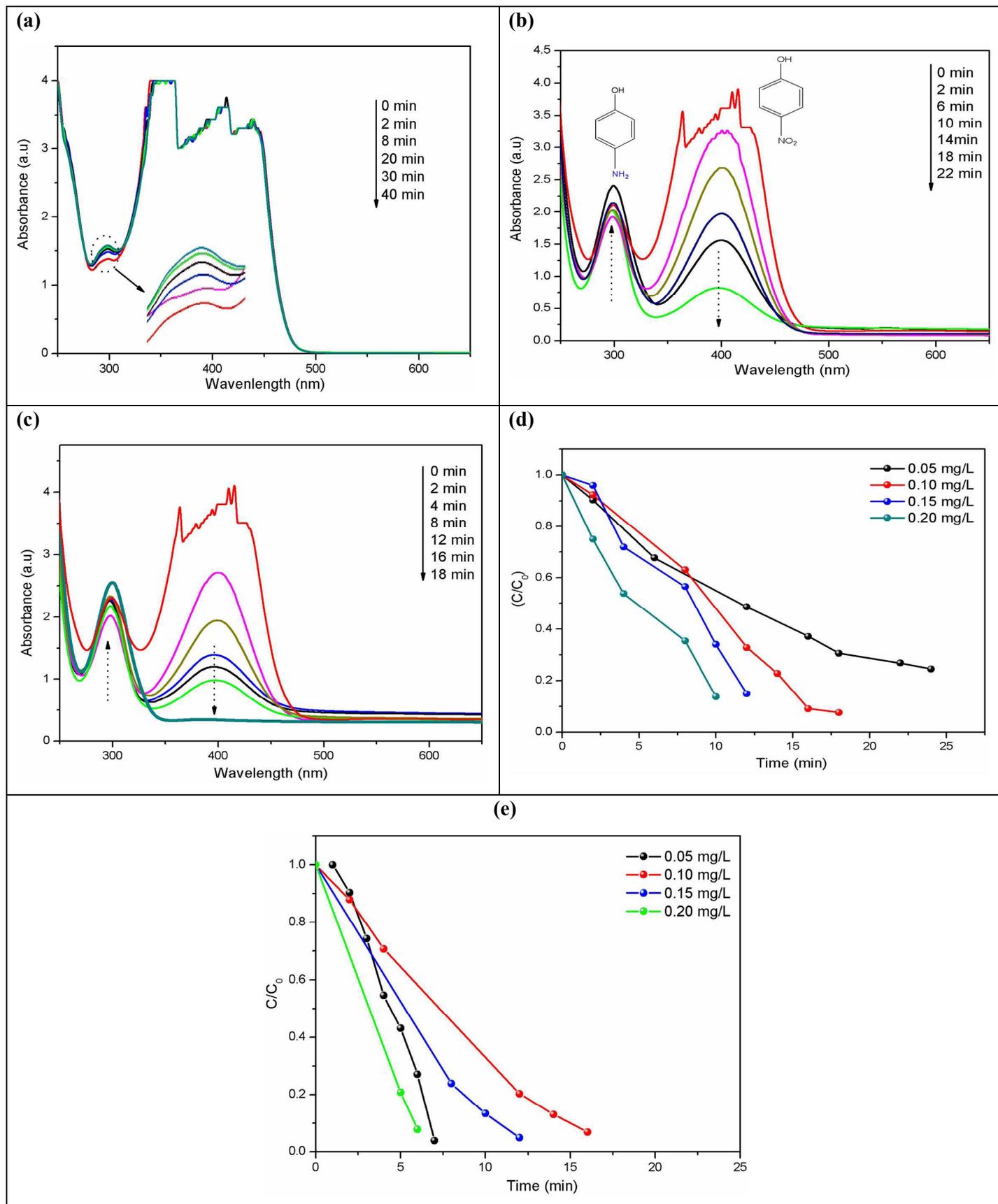
Fig. 8. UV–Vis absorption spectra for the reduction of 4-NP at room temperature with NaBH$_4$ (a), NaBH$_4$/CuO (b) and NaBH$_4$/CuO@Ag^0(c), effect of concentration CuO (d) and CuO@Ag^0 (e). Reaction conditions. 4-NP = 2.5mM, NaBH$_4$ = 0.2 M, [CuO]=0.05mg/L, [CuO@Ag^0]=0.05mg/L.

The C/C$_0$ value decreased down to ca. 0.12 after 10 min with 0.20 mg/L CuO concentration, but only to ca. 0.24 after 25 min with 0.05 mg/L CuO concentration. This indicates that a fourfold higher catalyst amount reduces by half the reaction time, and improves the 4-NP conversion from 76% to 88%. Less pronounced effect of the catalyst concentration was noticed with CuO@Ag^0, since almost similar C/C$_0$ ratio of ca. 0.2-0.5 were obtained after only 7-9 min of reaction. This result is of great importance, because it indicates that the influence of the catalyst amount, if any, should play only a minor role, and that the mere incorporation of AgNPs produces an almost total 4-NP reduction within half the time required for Ag-free CuO. Thus, it clearly appears that CuO enhance 4-NP reduction, and that CuO@Ag^0 display higher catalytic activity. Here, AgNPs must play a key role presumably by improving the electron transfer between already adsorbed reagents on CuO surface.

3.7. Kinetics of 4-NP reduction

Attempts to reaction kinetics taking into account that NaBH$_4$ has a much higher concentration as compared to 4-NP allowed using the pseudo first-order [32, 33]. The [instant /initial] absorbance ratio of the 4-NP band at 400 nm (A$_t$/A$_0$), which accounts for the corresponding concentration ratio (C$_t$/C$_0$), allows plotting ***ln(C$_t$/C$_0$)*** as a function of time (**Fig. S7**), according to equation 1.

$$Ln\frac{C_t}{C_0} = Ln\frac{A_t}{A_0} - k.t \qquad (1)$$

The linear evolution in time of $ln(C/C_0)$ confirms the 1st order kinetics for 4-NP reduction without and with catalyst, more particularly for relatively high catalyst concentrations, as

supported by R^2 values beyond 0.92 (**Table 1**). The mere addition of 0.05 mg/g of CuO or CuO@Ag^0 was found to induce a marked increase of the rate constant from 2.986 10^{-5} min^{-1} to 0.082 and 0.118 min^{-1} , respectively. This effect appears to be enhanced with increasing catalyst amount suggests that reagents adsorption is expected to play a significant role in the global process of 4-NP reduction, presumably by improving surface interaction between 4-NP molecules and BH$_4^-$anions [34]. The higher catalytic activity of CuO@Ag^0 as compared to CuO was somehow expected [35], and is supported by its higher rate constant ranging from 0.118 to 0.388 min^{-1} as compared to CuO for similar catalyst concentration (0.082 to 0.179 min^{-1}). Calculation of the 4-NP conversion yield as being (1-C_t/C_0) X 100% based on the UV-Vis absorbance at 400 nm (**Fig. S8)** revealed that high catalyst amounts of 0.20 mg/L produce high reduction yield of 90% and beyond in less than 10 min with CuO versus 5 min with CuO@Ag^0, in agreement with previous statements.

Table 1. First-order rate constants for the catalytic reduction of 4-NP at room temperature.

samples	Concentration (mg/L)	$k(min^{-1})$	R^2
CuO	0.05	0.082	0.893
	0.10	0.062	0.686
	0.15	0.103	0.970
	0.20	0.179	0.915
CuO@Ag^0	0.05	0.118	0.900
	0.10	0.163	0.994
	0.15	0.233	0.922
	0.20	0.388	0.989

K is the rate constant for the 1st order kinetics, and is expressed in min-1
R^2 is the correlation coefficient of the linear regression.

This enhancement of the catalytic properties is supposed to involve both reagents diffusion towards the solid surface, followed by adsorption and electron transfer not only on the metal surface but also on Ag^0-CuO interface [36]. The higher catalytic activity of CuO@Ag^0 contrasts with its lower specific surface area (8.03 m^2/g) and pore volume (0.013 cc/g) as compared to CuO (55.31 m^2/g and 0.124 cc/g, respectively). This suggests a higher surface reactivity for CuO@Ag^0 most likely due to the presence of AgNPs. The first order kinetics of

4-NP reduction indicates that the concentration of 4-NP is the key factor, and that the surface reaction is the rate-controlling step.

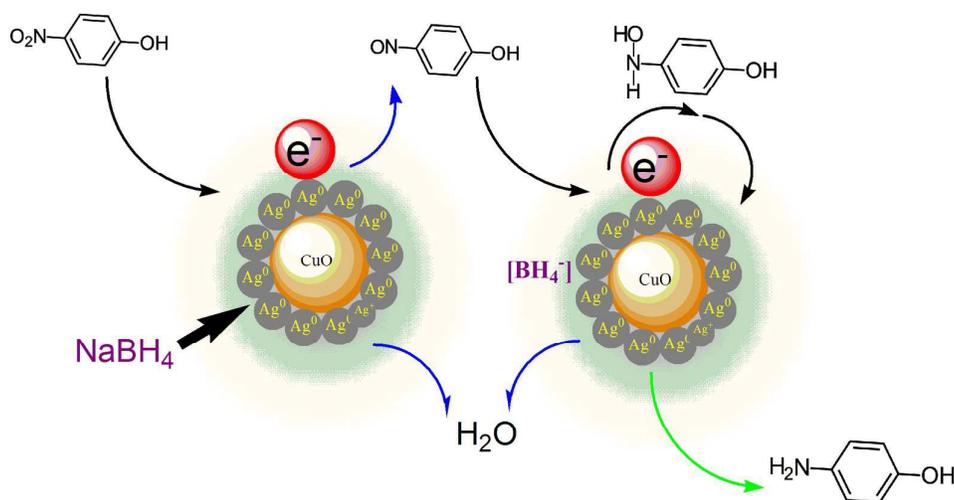### 3.8. Proposed mechanism for the catalytic properties improvements

As known, the presence of $NaBH_4$ in aqueous solution of 4-NP resulted in the deprotonation of 4-NP to nitrophenolate ions. The as-prepared CuO@Ag material with improved catalytic activity can be attributed to *(i)* the active Ag shell and a large adsorption of 4-nitrophenol reactants onto the positively-charged Ag-OH groups and *(ii)* to the accumulation of electrons charge on the CuO particle as core. At this regard, borohydride ions are adsorbed onto the surface of CuO@Ag to react and transfer electrons to the Ag-shell surface. Then, CuO-core have a tendency to attract electrons and act as electron acceptors. Thus charge distribution occurs between the copper oxide and silver particles. Here, electrons leave the Ag particles and end up with an electron enriched region at the interface of CuO-core. Meanwhile, the 4-nitrophenolate anion reactants can be easily adsorbed onto the positively charged CuO particles. Thus, existence of the surplus electrons added to the CuO facilitates the uptake of electrons by the adsorbed 4-nitrophenol molecules, which leads to the reduction of 4-NPs into the 4-aminophenol products. Detachment of the product 4-aminophenol creates a free surface.

According to the observed profile, the reduction can occur in several steps, the reaction proceeds into three steps: the very fast reduction of 4-NPs to 4-nitrophenol and then to 4-hydroxylaminophenol, which is reduced to the aminophenol in the final, slowest step.

Additionally, a significant confirmation was obtained from the decreased intensity of the peak at 400 nm. This decrease was caused by the continuous consumption of 4-NP and the reaction mechanism was causative as the inherent hydrogen was adsorbed by CuO layers, which transported the hydrogen between the $NaBH_4$ and the 4-NP.

According to the above results, it can be assumed that the first step involves $NaBH_4$ and 4-NP adsorption on the catalyst surface. This should promote electron transfer that triggers the

deprotonation of 4-NP into nitrophenolate ions (**Scheme 2**). AgNPs present on CuO surface

are expected to act as Lewis acidic species that attracts the electron pairs of the nitro group of

4-NP which behave as Lewis base (pka = 7.15 at 25). Thus, 4-NP adsorption should involve

$Ag:NO_2-$ interaction, which is consistent with the significant improvement of the catalyst

activity after AgNP incorporation. The continuous flux of electron due to $NaBH_4$ excess

should favor quick reduction of the adsorbed nitro groups into amino ones and the formation

of aminophenol through the formation intermediates such as hydroxylamine groups (4-HO-

(NO)Phenyl-OH) and/or oximes one (HO-N-Phenyl-OH). In both cases, the adsorbed water

should play a key role in hydrogen atom transfer and distribution of proton on the surface.

Nevertheless, the main issue to be addressed is what type of interactions are involved between

the inorganic catalyst with organic substrates in aqueous media.

Scheme 2. Proposed mechanism for 4-NP reduction with $CuO@Ag^0$ as catalyst.

The predominance of protons in the upper layer of the first water bilayer on bare metal

particle must contribute in supplying the required H atom for the formation of these

intermediates. This water bilayer is stabilized by the predominance of OH^- on the very surface

of Ag^0 [37]. The bare metal surface is supposed to attract water molecules, and paradoxically

the resulting water–metal interface becomes hydrophobic [38-40]. This explains somehow the

adsorption of organic molecules such as 4-NP on AgNPs, and thereby the catalytic activity improvement upon metal incorporation. Besides, silver is recognized as being the best electrical conductor $(6,30 \times 10^7 \text{ S} \cdot \text{m}^{-1})$ as compared to other metals such as copper, gold, aluminum, iron and even steel and carbon. This makes silver to behave a a bifunctional catalyst by favoring reagent adsorption and electron transfer. The high catalytic activity of Ag^0-CuO supposes that the desorption of the resulting 4-AP is fast. This can be explained in terms of quick protonation of the amino group of 4-AP and the rise of repulsion forces due to the predominance of protons in the external water layer around AgNPs [37]. Here, the size, morphology, electronic structure and surface area are key-factors in the catalytic activity of such materials [41, 42].

3.9. Catalytic stability

Repetitive catalytic tests revealed slight decrease of 3% of the catalytic activity after one turnover of the fresh catalyst and of ca. 15% after three turnovers (**Fig.9**). This was attributed to slight aggregation of AgNPs and structure alteration as supported by IR data (**Fig. S9**). This major shortcoming can be conveniently addressed by dispersing metal nanoparticles in CuO-supported organic moieties such amines, polyol or amino-polyol dendrimers. Research is still in progress in this direction.
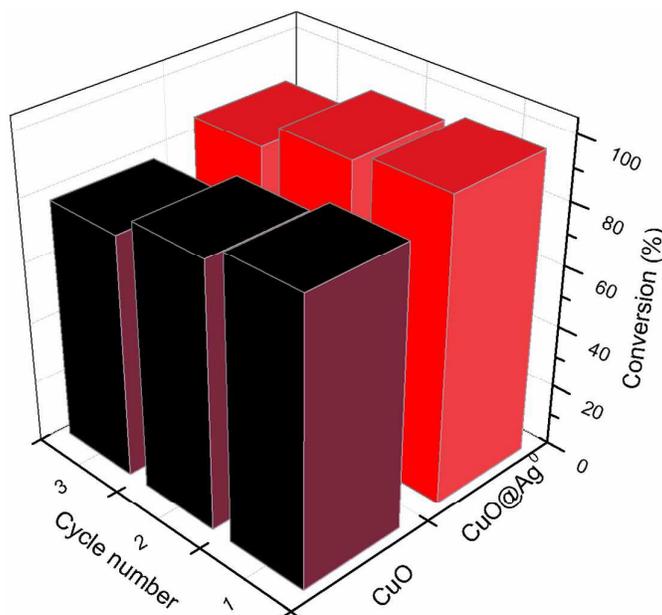
Fig.9. Conversion yield of 4-NP after repetitive catalytic tests of CuO and CuO@Ag^0 at room temperature. Reaction conditions. 4-NP = 2.5mM, NaBH$_4$ = 0.2 M, [CuO]=0.10 mg/L, [CuO@Ag^0]=0.10 mg/L.

3.10. Antibacterial activity

In parallel of 4-NP reduction, the antibacterial activities of CuO and CuO@Ag were evaluated by following the turbidity of the solution. Different concentrations (from 0.12 to 2 µg/mL) of nanoparticles were prepared and the effect on *S. aureus* was presented in **Fig. 10**. From these experiments, the prepared materials effectively inhibited bacterial growth and CuO@Ag^0 is observed to be more effective than CuO, due to their interesting properties. The obtained results revealed that MIC values registered for CuO@Ag^0 was in the range of 50 µg.mL^{-1}.

The difference on the antibacterial response can be explained in term that CuO encapsulated Ag^0-NPs is considered to be the result of the generation of reactive oxygen species, including superoxide (•O^{2-}) and hydrogen radical (•OH) from its surface. Firstly, the increase of the reactive oxygen species amount, produced by hydroxyl radicals and singlet oxygen [60, 61]. The second estimation was the implication of the nanoparticles on the surface of bacteria [62-70]. These results are in good agreement in both particle size and surface, as supported by

SEM, ZP and BET analysis. Also, this can be explained by the synergistic effect from hydrophilicity and electrostatic interaction between the CuO core and Ag^0-NPs shell surface. Thus, the contact between bacterium and nanoparticles was increased, which was in correlation by its good adsorption properties and/or surface area (8.03 m^2 /g).
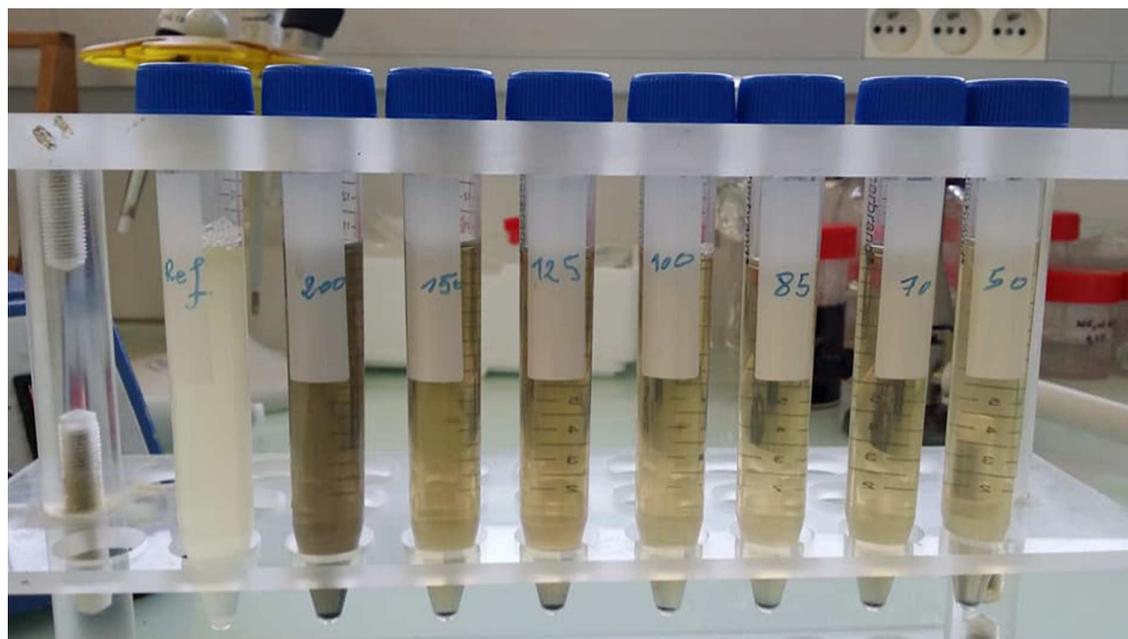
Figure. 10: Change in solution turbid for various concentration of $CuO@Ag^0$.

3.11. Destruction of bacterial cell wall

In order to explain how the damage of cell bacterial, upon contact with $CuO@Ag^0$ nanoparticles, a possible mechanism have been proposed to describe the antibacterial behavior, as follow. For this, after treatment with $CuO@Ag^0$, the amount of *S. aureus* greatly decreased, where the damage and leakage of intracellular contents could be occurred [71]. Herein, the leaking of intracellular could be explained in term of the direct interaction between materials nanoparticles and the external membrane surface of the bacteria.

At this regards, we suppose that antibacterial activities can be divided into two main parts according to the reaction between antibacterial samples and bacterial cells. Firstly, the cell membrane disruption, which was the key factor in the antibacterial activities. Secondly the

Dalton Transactions Accepted Manuscript

increases of bacterial growth are related to the particles size and generation of reactive oxygen species [72-74]. From the above results obtained in MIC, it can be assumed that the CuO@Ag^0 nanoparticles are effective in killing a wide range of bacterial growth. From Zetasizer and AFM analysis, CuO@Ag^0 are in smallest particles that likely create some attach to the bacteria and produce more reactive oxygen species [75, 76]. Thus, the reactive oxygen species becomes to interact with bacterial membrane cell. Afterwards, the reactive oxygen species can be penetr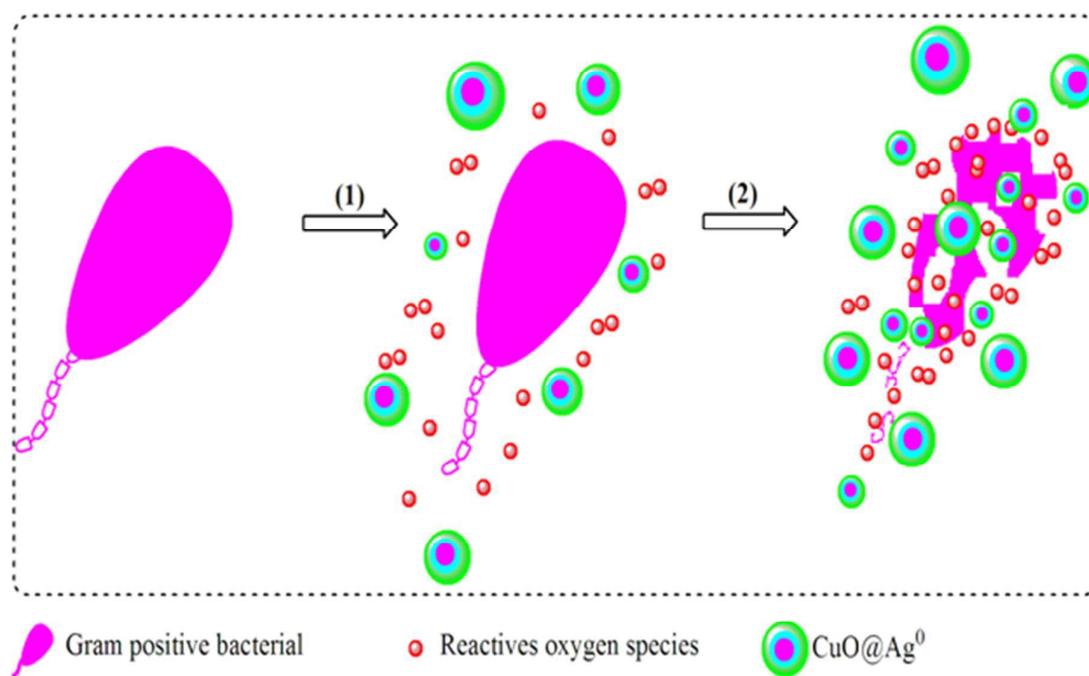ate to the individual core-shell-shell particles into the cell [77]. Here, the presence of CuO@Ag^0 nanoparticles leads to damages to the membrane wall of *S. aureus* (**Scheme.3**). This effect can be explained by the strong direct interactions with bacterial membrane surface and antibacterial agent like CuO@Ag^0. Based on these interesting results, the new CuO@Ag^0 core-shell could be employed as an efficient antibacterial material.

To check the viability of the *S. aureus* cells, further streaking was done from the evolution of the bacteria concentration during various times (**Fig.11**). Visible changes are marked after 2 hours incubation, suggesting the kicky effect of Cu@Ag nanoparticles. As expected, proper decreases were obtained for the bacteria concentration, and then merged to zero after 30 hours. Broadly, Ag nanoparticles appeared to be more effective bactericidal agents compared with CuO nanoparticles. Likely the smaller size of the Ag-shell enabled them to damage the cell envelope structural arrangement. Moreover, they could easily accumulate in both the periplasmic space and the cytosol, which in turn affected the structure and function of other biomolecules.
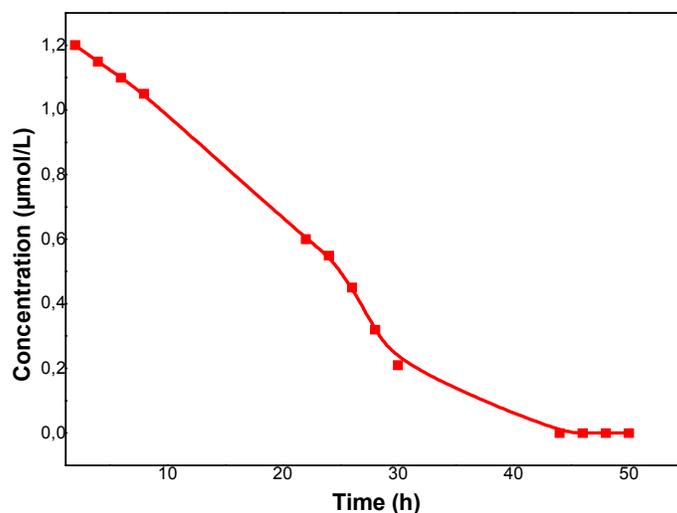
Fig.11: Growth curves of *S. aureus exposed to CuO@Ag core-shell.*

The presence of a thin peptidoglycan cell wall and an outer membrane make its envelope less rigid. Therefore, as depicted in **Scheme 3**, it is proposed that the CuO@Ag nanoparticles could be easily adsorbed on the cell surface leading to their gradual accumulation in the periplasmic space and other cellular compartments. CuO@Ag presents in the outer membrane cause a net negative charge on the surface of *S. aureus* cells. This multitude of adverse effects by the CuO@Ag resulted in the inhibition of *S. aureus* growth and cell death.

Dalton Transactions Accepted Manuscript

Legend:
- Gram positive bacterial
- Reactives oxygen species
- CuO@Ag^0

Scheme. 3: Schematic representation of antibacterial mechanism.

6. Conclusion

CuO@Ag^0 turned out to be an effective catalyst for 4-nitrophenol reduction into 4-aminophenol and antibacterial agent at room temperature. Ag nanoparticles incorporation produced a structure compaction due to metal interaction with the terminal CuOH groups. The first step of the investigated process appears to involve previous reactant adsorption on the catalyst surface trough Ag:NO$_2$- interaction. The water adsorbed on the bare metal surface should play a key role in supplying the required H atom for the formation of reaction intermediates and in inducing sufficiently hydrophobic character that improves 4-NP adsorption and simultaneously repulsion force that favor the desorption of protonated 4-AP. Additionally, it was found that the surface area, stability and chemical composition of CuO@Ag^0 were the most important factors affecting the antibacterial activity of this material. This implies the proficient antibacterial activity of CuO against *S. aureus*. The structure

stability of CuO@Ag^0 can be improved by incorporation metal stabilizing agent and investigations are still in progress in this direction.

References:

1. Thavasi, V., G. Singh, and S. Ramakrishna, *Electrospun nanofibers in energy and environmental applications.* Energy & Environmental Science, 2008. **1**(2): p. 205-221.
2. Liu, L., et al., *Adsorption removal of dyes from single and binary solutions using a cellulose-based bioadsorbent.* ACS Sustainable Chemistry & Engineering, 2015. **3**(3): p. 432-442.
3. Magaraggia, M., et al., *Porphyrin–silica microparticle conjugates as an efficient tool for the photosensitised disinfection of water contaminated by bacterial pathogens.* Photochemical & Photobiological Sciences, 2013. **12**(12): p. 2170-2176.
4. Ghasemi, N., F. Jamali-Sheini, and R. Zekavati, *CuO and Ag/CuO nanoparticles: Biosynthesis and antibacterial properties.* Materials Letters, 2017. **196**: p. 78-82.
5. Zhang, J., et al., *Highly active PtAu alloy nanoparticle catalysts for the reduction of 4-nitrophenol.* Nanoscale, 2014. **6**(4): p. 2125-2130.
6. Zhao, P., et al., *Basic concepts and recent advances in nitrophenol reduction by gold-and other transition metal nanoparticles.* Coordination Chemistry Reviews, 2015. **287**: p. 114-136.
7. Lee, S.-Y. and S.-J. Park, *TiO 2 photocatalyst for water treatment applications.* Journal of Industrial and Engineering Chemistry, 2013. **19**(6): p. 1761-1769.
8. Sambandam, B., et al., *Rapid synthesis of C-TiO2: tuning the shape from spherical to rice grain morphology for visible light photocatalytic application.* ACS Sustainable Chemistry & Engineering, 2015. **3**(7): p. 1321-1329.
9. Lüddeke, F., et al., *Removal of total and antibiotic resistant bacteria in advanced wastewater treatment by ozonation in combination with different filtering techniques.* Water research, 2015. **69**: p. 243-251.
10. Qu, X., et al., *Nanotechnology for a safe and sustainable water supply: enabling integrated water treatment and reuse.* Accounts of chemical research, 2012. **46**(3): p. 834-843.
11. Khajeh, M., S. Laurent, and K. Dastafkan, *Nanoadsorbents: classification, preparation, and applications (with emphasis on aqueous media).* Chemical reviews, 2013. **113**(10): p. 7728-7768.
12. Kyzas, G.Z. and K.A. Matis, *Nanoadsorbents for pollutants removal: a review.* Journal of Molecular Liquids, 2015. **203**: p. 159-168.
13. Decher, G., *Fuzzy nanoassemblies: toward layered polymeric multicomposites.* science, 1997. **277**(5330): p. 1232-1237.
14. Sun, Shaodong, et al. "Hollow Cu x O (x= 2, 1) micro/nanostructures: synthesis, fundamental properties and applications." *CrystEngComm* 19.42 (2017): 6225-6251.
15. Wu, Meng-Ke, et al. "High-performance supercapacitors of Cu-based porous coordination polymer nanowires and the derived porous CuO nanotubes." *Dalton Transactions* 46.48 (2017): 16821-16827.16.
16. Feng, Feng, Muzi Chen, and Ji Hong Wu. "Morphology-selective synthesis of Cu (NO 3) 2· 2.5 H 2 O micro/nanostructures achieved by rational manipulation of nucleation pathways and their morphology-preserved conversion to CuO porous micro/nanostructures." *CrystEngComm* 20.12 (2018): 1731-1738.

17. Singh, S., K. Barick, and D. Bahadur, *Functional oxide nanomaterials and nanocomposites for the removal of heavy metals and dyes.* Nanomaterials and Nanotechnology, 2013. **3**: p. 20.

18. Malwal, D. and P. Gopinath, *Enhanced photocatalytic activity of hierarchical three dimensional metal oxide@ CuO nanostructures towards the degradation of Congo red dye under solar radiation.* Catalysis Science & Technology, 2016. **6**(12): p. 4458-4472.

19. Hwang, S.H., et al., *Electrospun ZnO/TiO 2 composite nanofibers as a bactericidal agent.* Chemical Communications, 2011. **47**(32): p. 9164-9166.

20. Malwal, D. and P. Gopinath, *Fabrication and characterization of poly (ethylene oxide) templated nickel oxide nanofibers for dye degradation.* Environmental Science: Nano, 2015. **2**(1): p. 78-85.

21. Ragavan, K. and N.K. Rastogi, *Graphene–copper oxide nanocomposite with intrinsic peroxidase activity for enhancement of chemiluminescence signals and its application for detection of Bisphenol-A.* Sensors and Actuators B: Chemical, 2016. **229**: p. 570-580.

22. Alswat, A.A., M.B. Ahmad, and T.A. Saleh, *Zeolite modified with copper oxide and iron oxide for lead and arsenic adsorption from aqueous solutions.* Journal of Water Supply: Research and Technology-Aqua, 2016. **65**(6): p. 465-479.

23. Athar, S. and H. Asilian, *Catalytic oxidation of carbon monoxide using copper-zinc mixed oxide nanoparticles supported on diatomite.* Health Scope, 2012. **1**(2): p. 52-56.

24. Saleh, T.A., M.M. Al-Shalalfeh, and A.A. Al-Saadi, *Graphene Dendrimer-stabilized silver nanoparticles for detection of methimazole using Surface-enhanced Raman scattering with computational assignment.* Scientific Reports, 2016. **6**.

25. Yu, J., et al., *Preparation and photocatalytic activity of mesoporous anatase TiO 2 nanofibers by a hydrothermal method.* Journal of Photochemistry and Photobiology A: Chemistry, 2006. **182**(2): p. 121-127.

26. Shu, C., et al., *Synthesis of carbonated hydroxyapatite nanofibers by mechanochemical methods.* Ceramics international, 2005. **31**(1): p. 135-138.

27. Sharmila, G., M. Thirumarimurugan, and V.M. Sivakumar, *Optical, catalytic and antibacterial properties of phytofabricated CuO nanoparticles using Tecoma castanifolia leaf extract.* Optik-International Journal for Light and Electron Optics, 2016. **127**(19): p. 7822-7828.

28. Li, G., et al., *Role of surface/interfacial Cu2+ sites in the photocatalytic activity of coupled CuO– TiO2 nanocomposites.* The Journal of Physical Chemistry C, 2008. **112**(48): p. 19040-19044.

29. Afkhami, A. and R. Moosavi, *Adsorptive removal of Congo red, a carcinogenic textile dye, from aqueous solutions by maghemite nanoparticles.* Journal of Hazardous Materials, 2010. **174**(1): p. 398-403.

30. Bhattacharjee, A. and M. Ahmaruzzaman, *Green synthesis of 2D CuO nanoleaves (NLs) and its application for the reduction of p-nitrophenol.* Materials Letters, 2015. **161**: p. 79-82.

31. Mary, J.A., et al., *Microwave-assisted synthesis, characterization and antibacterial properties of Ce–Cu dual doped ZnO nanostructures.* Optik-International Journal for Light and Electron Optics, 2016. **127**(4): p. 2360-2365.

32. Pradhan, N., A. Pal, and T. Pal, *Silver nanoparticle catalyzed reduction of aromatic nitro compounds.* Colloids and Surfaces A: Physicochemical and Engineering Aspects, 2002. **196**(2): p. 247-257.

33. Choi, I., et al., *pH-controlled exponential and linear growing modes of layer-by-layer assemblies of star polyelectrolytes.* Journal of the American Chemical Society, 2011. **133**(24): p. 9592-9606.

34. Saeb, A., et al., *Production of silver nanoparticles with strong and stable antimicrobial activity against highly pathogenic and multidrug resistant bacteria.* The Scientific World Journal, 2014. **2014**.

35. Kim, H.J., I.C. Bang, and J. Onoe, *Characteristic stability of bare Au-water nanofluids fabricated by pulsed laser ablation in liquids.* Optics and Lasers in Engineering, 2009. **47**(5): p. 532-538.

36. Zhu, D., et al., *Dispersion behavior and thermal conductivity characteristics of Al 2 O 3–H 2 O nanofluids.* Current Applied Physics, 2009. **9**(1): p. 131-139.

37. Boldyrev, V., *Thermal decomposition of ammonium perchlorate.* Thermochimica Acta, 2006. **443**(1): p. 1-36.

38. Sharma, J., et al., *Catalytic thermal decomposition of ammonium perchlorate and combustion of composite solid propellants over green synthesized CuO nanoparticles.* Thermochimica Acta, 2015. **614**: p. 110-115.

39. Yan, Z., et al., *In situ loading of highly-dispersed CuO nanoparticles on hydroxyl-group-rich SiO 2-AlOOH composite nanosheets for CO catalytic oxidation.* Chemical Engineering Journal, 2017. **316**: p. 1035-1046.

40. Zhang, K., et al., *Development of a nano-Al⁄ Cu O based energetic material on silicon substrate.* Applied Physics Letters, 2007. **91**(11): p. 113117.

41. Kareem, T.A. and A.A. Kaliani, *Synthesis and thermal study of octahedral silver nano-plates in polyvinyl alcohol (PVA).* Arabian Journal of Chemistry, 2011. **4**(3): p. 325-331.

42. Nyquist, R.A. and R.O. Kagel, *Handbook of infrared and raman spectra of inorganic compounds and organic salts: infrared spectra of inorganic compounds*. Vol. 4. 2012: Academic press.

43. Walter, D., *Characterization of synthetic hydrous hematite pigments.* Thermochimica acta, 2006. **445**(2): p. 195-199.

44. Stoch, A., et al., *FTIR study of electrochemically deposited hydroxyapatite coatings on carbon materials.* Journal of Molecular Structure, 2003. **651**: p. 389-396.

45. Xu, Y., D. Chen, and X. Jiao, *Fabrication of CuO pricky microspheres with tunable size by a simple solution route.* The Journal of Physical Chemistry B, 2005. **109**(28): p. 13561-13566.

46. Panigrahi, S., et al., *Synthesis and size-selective catalysis by supported gold nanoparticles: study on heterogeneous and homogeneous catalytic process.* The Journal of Physical Chemistry C, 2007. **111**(12): p. 4596-4605.

47. Gangula, A., et al., *Catalytic reduction of 4-nitrophenol using biogenic gold and silver nanoparticles derived from Breynia rhamnoides.* Langmuir, 2011. **27**(24): p. 15268-15274.

48. Narayanan, K.B. and N. Sakthivel, *Synthesis and characterization of nano-gold composite using Cylindrocladium floridanum and its heterogeneous catalysis in the degradation of 4-nitrophenol.* Journal of hazardous materials, 2011. **189**(1): p. 519-525.

49. Kong, L., et al., *Constructing magnetic polyaniline/metal hybrid nanostructures using polyaniline/Fe 3 O 4 composite hollow spheres as supports.* Journal of Solid State Chemistry, 2009. **182**(8): p. 2081-2087.

50. Han, J., et al., *Fe 3 O 4/PANI/m-SiO 2 as robust reactive catalyst supports for noble metal nanoparticles with improved stability and recyclability.* Journal of Materials Chemistry A, 2014. **2**(32): p. 13016-13023.

51. Hervés, P., et al., *Catalysis by metallic nanoparticles in aqueous solution: model reactions.* Chemical Society Reviews, 2012. **41**(17): p. 5577-5587.

52. Geng, Q. and J. Du, *Reduction of 4-nitrophenol catalyzed by silver nanoparticles supported on polymer micelles and vesicles.* RSC Advances, 2014. **4**(32): p. 16425-16428.

53. Song, H., et al., *Hydrothermal growth of mesoporous SBA-15 silica in the presence of PVP-stabilized Pt nanoparticles: synthesis, characterization, and catalytic properties.* Journal of the American Chemical Society, 2006. **128**(9): p. 3027-3037.

54. Lu, H., et al., *Ultrafine silver nanoparticles with excellent antibacterial efficacy prepared by a handover of vesicle templating to micelle stabilization.* Polymer Chemistry, 2013. **4**(12): p. 3448-3452.

55. Esumi, K., R. Isono, and T. Yoshimura, *Preparation of PAMAM– and PPI– metal (silver, platinum, and palladium) nanocomposites and their catalytic activities for reduction of 4-nitrophenol.* Langmuir, 2004. **20**(1): p. 237-243.

56. Graetzel, M. and A.J. Frank, *Interfacial electron-transfer reactions in colloidal semiconductor dispersions. Kinetic analysis.* The Journal of Physical Chemistry, 1982. **86**(15): p. 2964-2967.

57. Chang, Y.-C. and D.-H. Chen, *Catalytic reduction of 4-nitrophenol by magnetically recoverable Au nanocatalyst.* Journal of hazardous materials, 2009. **165**(1): p. 664-669.

58. Lin, F.-h. and R.-a. Doong, *Highly efficient reduction of 4-nitrophenol by heterostructured gold-magnetite nanocatalysts.* Applied Catalysis A: General, 2014. **486**: p. 32-41.

59. Hao, Y., et al., *Mesoporous TiO 2 nanofibers with controllable Au loadings for catalytic reduction of 4-nitrophenol.* Materials Science in Semiconductor Processing, 2015. **40**: p. 621-630.

60. Yang, H., et al., *Comparative study of cytotoxicity, oxidative stress and genotoxicity induced by four typical nanomaterials: the role of particle size, shape and composition.* Journal of applied Toxicology, 2009. **29**(1): p. 69-78.

61. Zhang, L., et al., *Investigation into the antibacterial behaviour of suspensions of ZnO nanoparticles (ZnO nanofluids).* Journal of Nanoparticle Research, 2007. **9**(3): p. 479-489.

62. Storz, G. and J.A. Imlayt, *Oxidative stress.* Current opinion in microbiology, 1999. **2**(2): p. 188-194.

63. Kora, A.J. and J. Arunachalam, *Assessment of antibacterial activity of silver nanoparticles on Pseudomonas aeruginosa and its mechanism of action.* World Journal of Microbiology and Biotechnology, 2011. **27**(5): p. 1209-1216.

64. Morita, K., et al., *Thermally and chemically stable mixed valence copper oxide cluster ions revealed by post heating.* The Journal of Physical Chemistry A, 2013. **117**(40): p. 10145-10150.

65. Kim, J.-H., et al., *Effects of metal ions on the activity of protein tyrosine phosphatase VHR: highly potent and reversible oxidative inactivation by Cu 2+ ion.* Archives of Biochemistry and Biophysics, 2000. **382**(1): p. 72-80.

66. Sondi, I. and B. Salopek-Sondi, *Silver nanoparticles as antimicrobial agent: a case study on E. coli as a model for Gram-negative bacteria.* Journal of colloid and interface science, 2004. **275**(1): p. 177-182.

67. Azam, A., et al., *Size-dependent antimicrobial properties of CuO nanoparticles against Gram-positive and-negative bacterial strains.* Int J Nanomedicine, 2012. **7**(9): p. 3527-3535.

68. Yu-sen, E.L., et al., *Inactivation of Mycobacterium avium by copper and silver ions.* Water Research, 1998. **32**(7): p. 1997-2000.

69. Panáček, A., et al., *Silver colloid nanoparticles: synthesis, characterization, and their antibacterial activity.* The Journal of Physical Chemistry B, 2006. **110**(33): p. 16248-16253.

70. Tong, G., et al., *Antibacterial effects of the Cu (II)-exchanged montmorillonite on Escherichia coli K88 and Salmonella choleraesuis.* Veterinary microbiology, 2005. **105**(2): p. 113-122.

71. Yin, S., et al., *Functional Free-Standing Graphene Honeycomb Films.* Advanced Functional Materials, 2013. **23**(23): p. 2972-2978.

72. Chua, P.-H., et al., *Surface functionalization of titanium with hyaluronic acid/chitosan polyelectrolyte multilayers and RGD for promoting osteoblast functions and inhibiting bacterial adhesion.* Biomaterials, 2008. **29**(10): p. 1412-1421.

73. Kingshott, P., et al., *Covalent attachment of poly (ethylene glycol) to surfaces, critical for reducing bacterial adhesion.* Langmuir, 2003. **19**(17): p. 6912-6921.

74. Makhluf, S., et al., *Microwave-Assisted Synthesis of Nanocrystalline MgO and Its Use as a Bacteriocide.* Advanced Functional Materials, 2005. **15**(10): p. 1708-1715.

75. Hans, M., et al., *Role of copper oxides in contact killing of bacteria.* Langmuir, 2013. **29**(52): p. 16160-16166.

76. Applerot, G., et al., *Understanding the antibacterial mechanism of CuO nanoparticles: revealing the route of induced oxidative stress.* Small, 2012. **8**(21): p. 3326-3337.

77. Zhang, L., et al., *Mechanistic investigation into antibacterial behaviour of suspensions of ZnO nanoparticles against E. coli.* Journal of Nanoparticle Research, 2010. **12**(5): p. 1625-1636.

Graphical abstract :